Hindawi
Shock and Vibration
Volume 2022, Article ID 4161470, 18 pages
https://doi.org/10.1155/2022/4161470

Research Article

Effects of Resonator Shape on Nonlinear Resonant Frequencies of a Microresonant Pressure Sensor

Guang Han[1,2] and Lizhong Xu[1]

[1]*Yanshan University, Mechanical Engineering Institute, Qinhuangdao 066004, China*
[2]*Hebei Construction Material Vocational and Technical College, Electromechanical Engineer-ing Department, Qinhuangdao 066004, China*

Correspondence should be addressed to Lizhong Xu; xlz@ysu.edu.cn

Received 18 March 2022; Revised 25 August 2022; Accepted 7 September 2022; Published 17 October 2022

Academic Editor: Agustin Herrera-May

A nonlinear dynamics equation for a novel microresonant pressure sensor with a cross-type resonator is proposed. The nonlinear resonant frequencies of the sensor are calculated. Effects of the system parameters and gas pressure on the nonlinear resonant frequencies are investigated. Results show that the effects of nonlinearity on the resonant frequencies increase with increasing length of the resonator, and they decrease with decreasing the clearance between the resonator and the baseplate or gas pressure.

1. Introduction

Microelectromechanical systems (MEMS), with the advantages of high integration, high precision, low power consumption, and easy mass production, are widely used in intelligent manufacturing, robotics, and other fields [1–4]. MEMS include microsensors, microactuators, and processing circuits [5]. Among them, microsensors have been most widely studied [6].

Pressure microsensors are the most mature MEMS devices at present [7]. In the 1960s, the first micro pressure sensor was manufactured using micromachining technology [8]. In the 21st century, the micropressure sensor has developed rapidly. In 2001, Lange used metal oxide semiconductor technology and micromachining technology to produce a microsystem containing sensors with all necessary drives and signal conditioning circuits [9]. Werner and Fahrner used a diamond as a pressing die in a pressure sensor, allowing it to work in a high temperature environment around 300°C [10]. Han et al. proposed a high-precision resonant pressure sensor with two similar resonators; a linear fitting method was used to ensure its output linearity [11]. Li et al. developed a high-sensitivity resonant pressure microsensor, which included a sensing unit made of a silicon-on-insulator (SOI) wafer that was encapsulated by silicon glass, thus improving the conversion efficiency of pressure differences [12]. Shi et al. studied a microresonant pressure sensor with a pair of double-ended tuning forks as resonators [13]. Li et al. proposed a graphene-based resonant pressure sensor, which had the advantages of both a micromechanical sensor and a fiber resonator [14]. Matej et al. studied a ceramic resonant pressure sensor for working at high temperature (up to a maximum temperature of 201°C) [15]. Zhang et al. introduced a micromechanical resonant pressure sensor with two resonators and solved the overload problem [16]. Xiang et al. introduced a resonant pressure microsensor in which the silicon islands are deployed on an SOI wafer to improve the equivalent stiffness and structural stability of the pressure-sensitive diaphragm [17]. Zhao et al. and Yan et al. developed temperature-insensitive silicon resonant pressure sensors with very-low-frequency temperature coefficients [18, 19]. Zamanzadeh et al. proposed a resonant pressure sensor that provided a wider range of tunability and sensing range and a simplified signal-processing circuit [20]. Han et al. developed a new type of resonant pressure sensor based on electrostatic excitation and piezoresistive detection that had a measuring sensitivity of approximately 19 Hz/kPa [21]. Mata-Hernandez et al. introduced a resonant pressure sensor based on CMOS

technology and investigated its resonant frequency and quality factor [22]. Alcheikh et al. proposed a kind of resonant pressure sensor with high sensitivity whose sensitivity was significantly improved by switching between its first and third modes [23].

As the summary above suggests, numerous studies of microresonant pressure sensors have been completed. Among them, the capacitance-detection technique is easy to implement and is widely used. However, the capacitance between the resonator and the base is very small, so the capacitance change signal in resonance is small, which increases the difficulty of producing the subsequent amplifier circuit. For it, this paper proposes a microresonant pressure sensor with a cross-type resonator to increase the area in the middle of the resonator. It can increase capacitance between the resonator and the base to increase the capacitance change signal in resonance [24].

The resonator is an important component of the microresonant pressure sensor. Research on the resonant vibration of the resonator is significant for the design and application of the pressure sensor. Li et al. investigated nonlinear dynamics of a resonant silicon bridge pressure sensor with electrothermal excitation [25]. Zhang et al. studied the resonant frequency of the interfering mode for a resonant pressure sensor and separated it well away from the operational mode [26]. Fu and Xu proposed a multifield coupled dynamics model of a microresonant pressure sensor and studied the influence of various factors on the nonlinear vibration of the sensor [27, 28]. However, for the microresonant pressure sensor with a cross-type resonator, the nonlinear resonant frequencies have not yet been investigated.

In this paper, a nonlinear dynamics equation for a microresonant pressure sensor with a cross-type resonator is proposed. The nonlinear resonant frequencies of the microresonant sensor are calculated by using this equation with the multiscale method. Effects of system parameters and gas pressure on the nonlinear resonant frequencies are investigated. Our research results can be used to aid in design of the dynamic performance of microresonant pressure sensors.

First, a nonlinear vibration equation of the microresonant pressure sensor is proposed. Second, the vibration equation is solved using the multiscale method, and the nonlinear resonance frequency equation of the sensor is given. Third, changes of the nonlinear resonance frequency of the sensor are analyzed and discussed. At last, a conclusion is given.

2. Nonlinear Dynamics Equation of a Pressure Sensor

The coupled dynamics model of the microresonant pressure sensor is shown in Figure 1. Here, x is the coordinate of the central axis of the resonator; y is the position coordinate in the direction perpendicular to the x-axis; y (x, t) is the displacement of the resonator in the y-axis direction; L is half the length of the resonator; h is the thickness of the resonator; b is the width of the resonator; L_e and b_e are, respectively, the length and width of the cross structure on the resonator; d_0 is the initial clearance between the resonator and the baseplate; q (x, t) is the force per unit length applied to the resonator; U_0 is the voltage between the resonator and the baseplate.

The dynamics equation of the resonator is [29].

$$EI\frac{\partial^4 y(x,t)}{\partial x^4} - F\frac{\partial^2 y(x,t)}{\partial x^2} + \rho S\frac{\partial^2 y(x,t)}{\partial t^2} + C_a\frac{\partial y(x,t)}{\partial t} = q(x,t), \tag{1}$$

where E is the modulus of elasticity; I is the second moment; F is the inner axial force of the resonator; ρ is the density of the resonator material; S is the cross-sectional area of the resonator; C_a is the gas damping factor: $C_a = \eta b^3/(d_0 - y)^3$ (η is the dynamic viscosity of the gas).

The gas damping force per unit length is [30].

$$f_p = C_a\frac{\partial y}{\partial t}. \tag{2}$$

The displacement y (x, t) includes two parts: static displacement y_0 and dynamic displacement Δy. The damping force can be written as a Taylor series at $y = y_0$, which is given as follows:

$$f_p = \frac{\eta b^3}{(d_0 - y_0)^3}\frac{\partial \Delta y}{\partial t} + \frac{3\eta b^3}{(d_0 - y_0)^4}\Delta y\frac{\partial \Delta y}{\partial t} + \frac{6\eta b^3}{(d_0 - y_0)^5}\Delta y^2\frac{\partial \Delta y}{\partial t} + \frac{10\eta b^3}{(d_0 - y_0)^6}\Delta y^3\frac{\partial \Delta y}{\partial t} + \cdots. \tag{3}$$

The higher-order terms above the third order are omitted; Eq. (3) can be rewritten as

$$f_p = c_{Op0}\frac{\partial \Delta y}{\partial t} + c_{Op1}\Delta y\frac{\partial \Delta y}{\partial t} + c_{Op2}\Delta y^2\frac{\partial \Delta y}{\partial t} + c_{Op3}\Delta y^3\frac{\partial \Delta y}{\partial t}, \tag{4}$$

where $c_{Op0} = \eta b^3/(d_0 - y_0)^3$; $c_{Op1} = 3\eta b^3/(d_0 - y_0)^4$; $c_{Op2} = 6\eta b^3/(d_0 - y_0)^5$; $c_{Op3} = 10\eta b^3/(d_0 - y_0)^6$.

If $\varepsilon = y_0/d_0$ is defined as the nonlinear parameter, we have

$$\begin{aligned} c_{Op0} &= \frac{\eta b^3}{(d_0 - y_0)^3} \\ &= \frac{\eta b^3}{d_0^2 y_0}\frac{y_0}{d_0}\left[1 + \frac{y_0}{d_0} + \left(\frac{y_0}{d_0}\right)^2 + \right]^3 \\ &\approx \varepsilon\frac{\eta b^3}{d_0^2 y_0} = \varepsilon c_{p0}, \end{aligned} \tag{5a}$$

$$\begin{aligned} c_{Op1} &= \frac{3\eta b^3}{(d_0 - y_0)^4} \\ &= \frac{3\eta b^3}{d_0^3 y_0}\frac{y_0}{d_0}\left[1 + \frac{y_0}{d_0} + \left(\frac{y_0}{d_0}\right)^2 + \cdots\right]^4 \\ &\approx \varepsilon\frac{3\eta b^3}{d_0^3 y_0} = \varepsilon c_{p1}, \end{aligned} \tag{5b}$$

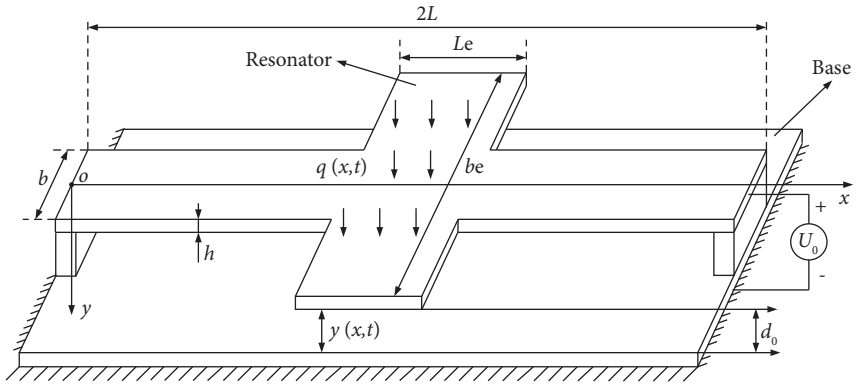

Figure 1: Coupled dynamics model of the sensor.

$$c_{Op2} = \frac{6\eta b^3}{(d_0 - y_0)^5} = \frac{6\eta b^3}{d_0^4 y_0}\frac{y_0}{d_0}\left[1 + \frac{y_0}{d_0} + \left(\frac{y_0}{d_0}\right)^2 + \cdots\right]^5 \approx \varepsilon\frac{6\eta b^3}{d_0^4 y_0} = \varepsilon c_{p2}, \tag{5c}$$

$$c_{Op3} = \frac{10\eta b^3}{(d_0 - y_0)^6} = \frac{10\eta b^3}{d_0^5 y_0}\frac{y_0}{d_0}\left[1 + \frac{y_0}{d_0} + \left(\frac{y_0}{d_0}\right)^2 + \cdots\right]^6 \approx \varepsilon\frac{10\eta b^3}{d_0^5 y_0} = \varepsilon c_{p3}. \tag{5d}$$

Let Δq denote the dynamic force per unit length of the resonator along the x-axis; it includes the dynamic electric force Δq_0 and the dynamic van der Waals force Δq_r:

$$\Delta q = \Delta q_0 + \Delta q_r. \tag{6}$$

The Van der Waals force per unit length of the resonator is [31].

$$f_v = \frac{H_v}{6\pi}\frac{b}{(d_0 - y)^3}, \tag{7}$$

where H_V is the Hamaker constant: $H_V = 10^{-19}$J.

The Van der Waals force can also be written as a Taylor series at $y = y_0$:

$$f_v = \frac{H_v}{6\pi}\frac{b}{(d_0 - y_0)^3} + \frac{H_v}{2\pi}\frac{b}{(d_0 - y_0)^4}\Delta y + \frac{H_v}{\pi}\frac{b}{(d_0 - y_0)^5}\Delta y^2 + \frac{5H_v}{3\pi}\frac{b}{(d_0 - y_0)^6}\Delta y^3 + \cdots. \tag{8}$$

Here, the static Van der Waals force is

$$f_{v0} = \frac{H_v}{6\pi}\frac{b}{(d_0 - y_0)^3}. \tag{9}$$

The higher-order terms above the third order are omitted, and the dynamic Van der Waals force can be expressed as follows:

$$\Delta q_r = k_{vs1}\Delta y + k_{vs2}\Delta y^2 + k_{vs3}\Delta y^3 \tag{10}$$

where

$$k_{vs1} = \frac{H_v}{2\pi}\frac{b}{(d_0 - y_0)^4} = \frac{H_v}{2\pi}\frac{b}{d_0^3 y_0}\frac{y_0}{d_0}\left[1 + \frac{y_0}{d_0} + \left(\frac{y_0}{d_0}\right)^2 + \cdots\right]^4 \approx \varepsilon\frac{H_v}{2\pi}\frac{b}{d_0^3 y_0}$$

$$k_{vs2} = \frac{H_v}{\pi}\frac{b}{(d_0 - y_0)^5} = \frac{H_v}{\pi}\frac{b}{d_0^4 y_0}\frac{y_0}{d_0}\left[1 + \frac{y_0}{d_0} + \left(\frac{y_0}{d_0}\right)^2 + \cdots\right]^5 \approx \varepsilon\frac{H_v}{\pi}\frac{b}{d_0^4 y_0}, \tag{11}$$

$$k_{vs3} = \frac{5H_v}{3\pi}\frac{b}{(d_0 - y_0)^6} = \frac{5H_v}{3\pi}\frac{b}{d_0^4 y_0^2}\left(\frac{y_0}{d_0}\right)^2\left[1 + \frac{y_0}{d_0} + \left(\frac{y_0}{d_0}\right)^2 + \cdots\right]^6 \approx \varepsilon\frac{5H_v}{3\pi}\frac{b}{d_0^5 y_0}.$$

The electric force per unit length of the resonator is [32].

$$f_e = \frac{1}{2}\frac{\varepsilon_o\varepsilon_r b U^2}{(d_0 - y)^2}. \tag{12}$$

It can also be written as a Taylor series at $y = y_0$:

$$f_e = \frac{\varepsilon_o \varepsilon_r b}{2(d_0 - y_0)^2} U^2 + \frac{\varepsilon_o \varepsilon_r b}{(d_0 - y_0)^3} U^2 \Delta y + \frac{3\varepsilon_o \varepsilon_r b}{2(d_0 - y_0)^4} U^2 \Delta y^2 + \frac{2\varepsilon_o \varepsilon_r b}{(d_0 - y_0)^5} U^2 \Delta y^3 + \cdots. \tag{13}$$

Here, the static electric force is

$$f_{e0} = \frac{\varepsilon_o \varepsilon_r b}{2(d_0 - y_0)^2} U^2. \tag{14}$$

The higher-order terms above the third order are omitted, and the dynamic electric force can be written as follows:

$$\Delta q_0 = \frac{\varepsilon_o \varepsilon_r b}{(d_0 - y_0)^3} U^2 \Delta y + \frac{3\varepsilon_o \varepsilon_r b}{2(d_0 - y_0)^4} U^2 \Delta y^2 + \frac{2\varepsilon_o \varepsilon_r b}{(d_0 - y_0)^5} U^2 \Delta y^3, \tag{15}$$

where ε_o is the vacuum permittivity; ε_r is the relative permittivity;

$$\begin{aligned} \frac{\varepsilon_o \varepsilon_r b}{(d_0 - y_0)^3} &= \frac{\varepsilon_o \varepsilon_r b}{d_0^2 y_0} \frac{y_0}{d_0} \left[1 + \frac{y_0}{d_0} + \left(\frac{y_0}{d_0}\right)^2 + \cdots\right]^3 \\ &\approx \varepsilon \frac{\varepsilon_o \varepsilon_r b}{d_0^2 y_0}, \\ \frac{3\varepsilon_o \varepsilon_r b}{2(d_0 - y_0)^4} &= \frac{3\varepsilon_o \varepsilon_r b}{2d_0^3 y_0} \frac{y_0}{d_0} \left[1 + \frac{y_0}{d_0} + \left(\frac{y_0}{d_0}\right)^2 + \cdots\right]^4 \\ &\approx \varepsilon \frac{3\varepsilon_o \varepsilon_r b}{2d_0^3 y_0}, \\ \frac{2\varepsilon_o \varepsilon_r b}{(d_0 - y_0)^5} &= \frac{2\varepsilon_o \varepsilon_r b}{d_0^4 y_0} \frac{y_0}{d_0} \left[1 + \frac{y_0}{d_0} + \left(\frac{y_0}{d_0}\right)^2 + \cdots\right]^5 \\ &\approx \varepsilon \frac{2\varepsilon_o \varepsilon_r b}{d_0^4 y_0}. \end{aligned} \tag{16}$$

Substituting Eqs. (10) and (15) into Eq. (6) yields

$$\Delta q = \varepsilon \xi_1 \Delta y + \varepsilon \xi_2 \Delta y^2 + \varepsilon \xi_3 \Delta y^3, \tag{17}$$

where $\xi_1 = (\varepsilon_o \varepsilon_r b U^2 / d_0^2 y_0) + (H_v b / 2\pi d_0^3 y_0)$; $\xi_2 = (3\varepsilon_o \varepsilon_r b U^2 / 2d_0^3 y_0) + (H_v b / \pi d_0^4 y_0)$; $\xi_3 = (2\varepsilon_o \varepsilon_r b U^2 / d_0^4 y_0) + (5H_v b / 3\pi d_0^5 y_0)$.

Upon substituting Eqs. (4) and (17) into Eq. (1), the coupled dynamics equation of the microresonant pressure sensor is obtained as follows:

$$EI \frac{\partial^4 \Delta y}{\partial x^4} - F \frac{\partial^2 \Delta y}{\partial x^2} + \rho S \frac{\partial^2 \Delta y}{\partial t^2} + \varepsilon \left(c_{p0} + c_{p1} \Delta y + c_{p2} \Delta y^2 + c_{p3} \Delta y^3\right) \frac{\partial \Delta y}{\partial t} = \varepsilon \xi_1 \Delta y + \varepsilon \xi_2 \Delta y^2 + \varepsilon \xi_3 \Delta y^3. \tag{18}$$

3. Solution of Nonlinear Dynamics Equation

Letting $\Delta y = \phi(x) q(t)$ and substituting it into Eq.(18) yields

$$\frac{q''}{q} + \varepsilon \frac{q'}{\rho S} \left(\frac{c_{p0}}{q} + c_{p1} \overline{\phi} + c_{p2} \overline{\phi}^2 q + c_{p3} \overline{\phi}^3 q^2\right) - \frac{\varepsilon \xi_2 \overline{\phi} q}{\rho S} - \frac{\varepsilon \xi_3 \overline{\phi}^2 q^2}{\rho S} = \frac{F}{\rho S} \frac{\phi^{(2)}}{\phi} - \frac{EI}{\rho S} \frac{\phi^{(4)}}{\phi} + \frac{\varepsilon \xi_1}{\rho S}. \tag{19}$$

Setting the left and right sides of Eq. (19) to be equal to $-\omega^2$ yields

$$\phi^{(4)} - \frac{F}{EI} \phi^{(2)} - \left(\omega^2 \frac{\rho S}{EI} + \frac{\varepsilon \xi_1}{EI}\right) \phi = 0, \tag{20}$$

$$q'' + \omega^2 q + \varepsilon A_1 q' + \varepsilon A_2 q' q + \varepsilon A_3 q' q^2 + \varepsilon A_4 q' q^3 - \varepsilon A_5 q^2 - \varepsilon A_6 q^3 = 0, \tag{21}$$

where $A_1 = c_{p0}/\rho S$, $A_2 = c_{p1} \overline{\phi} / \rho S$, $A_3 = c_{p2} \overline{\phi}^2 / \rho S$, $A_4 = c_{p3} \overline{\phi}^3 / \rho S$, $A_5 = \xi_2 \overline{\phi} / \rho S$, and $A_6 = \xi_3 \overline{\phi}^2 / \rho S$.

$$\overline{\phi} = \frac{1}{L} \int_0^L |\phi(x)| \mathrm{d}x, \quad \overline{\phi}^2 = \frac{1}{L} \int_0^L |\phi(x)|^2 \mathrm{d}x, \quad \overline{\phi}^3 = \frac{1}{L} \int_0^L |\phi(x)|^3 \mathrm{d}x. \tag{22}$$

Eq.(20) can be changed into the following form:

$$\phi^{(4)}(x) - \alpha^2 \phi^{(2)}(x) - \beta^4 \phi(x) = 0, \tag{23}$$

where $\alpha^2 = F/EI$ and $\beta^4 = \omega^2 (\rho S / EI) + (\varepsilon \xi_1 / EI)$.

The four characteristic roots of Eq.(23) are

$$\begin{cases} s_{1,2} = \pm i\lambda_1 = \pm i\sqrt{-\dfrac{\alpha^2}{2} + \sqrt{\dfrac{\alpha^4}{4} + \beta^4}}, \\ s_{3,4} = \pm \lambda_2 = \pm \sqrt{\dfrac{\alpha^2}{2} + \sqrt{\dfrac{\alpha^4}{4} + \beta^4}}, \end{cases} \tag{24}$$

where $\lambda_1 = \sqrt{-(\alpha^2/2) + \sqrt{(\alpha^4/4) + \beta^4}}$ and $\lambda_2 = \sqrt{(\alpha^2/2) + \sqrt{(\alpha^4/4) + \beta^4}}$.

With two local coordinate system set up, the origins are located on the left and right ends of the resonator (see Figure 2). In the left coordinate system, the mode function of the left resonator is

$$\phi_1(x) = C_1 \mathrm{ch}\lambda_2 x + C_2 \mathrm{sh}\lambda_2 x + C_3 \cos\lambda_1 x + C_4 \sin\lambda_1 x. \tag{25}$$

In the right coordinate system, the mode function of the right resonator is

$$\phi_2(x) = C_5 \mathrm{ch}\lambda_2 x + C_6 \mathrm{sh}\lambda_2 x + C_7 \cos\lambda_1 x + C_8 \sin\lambda_1 x, \tag{26}$$

where the undetermined constants C_j ($j = 1, 2, 3, 4, 5, 6, 7,$ and 8) and the parameters $\lambda_j (j = 1, 2)$ can be determined by boundary conditions and continuity conditions.

Since the displacement and rotation angle at the fixed end of the resonator are zero, we have

$$\phi(0) = \phi'(0) = 0. \tag{27}$$

At the center of the resonator, there is a concentrated mass, so the shear force in the resonator is equal to the inertia force of the concentrated mass, i.e.,

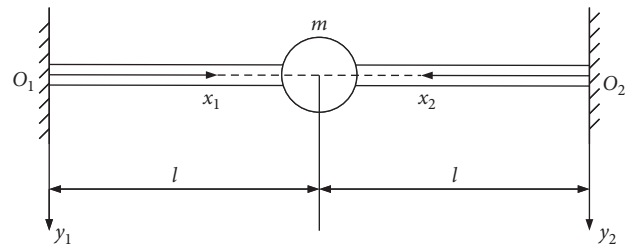

Figure 2: Coordinate systems for the resonator vibration analysis.

$$EI\phi'''(L) = -\frac{1}{2}m\omega^2\phi(L). \tag{28}$$

When the mode function of the left resonator is antisymmetric to the mode function of the right resonator, it can be concluded that

$$\begin{cases} \phi_1(0) = \phi_1(L) = 0, \\ \phi_1'(0) = 0, \\ EI\phi_1'''(L) = -\dfrac{1}{2}m\omega^2\phi_1(L). \end{cases} \tag{29}$$

When the mode function of the left resonator is symmetric to the mode function of the right resonator, we have, instead,

$$\begin{cases} \phi_1(0) = 0, \\ \phi_1'(0) = \phi_1'(L) = 0, \\ EI\phi_1'''(L) = -\dfrac{1}{2}m\omega^2\phi_1(L). \end{cases} \tag{30}$$

Substituting Eq.(25) into (29) yields

$$\begin{cases} C_1 + C_3 = 0, \\ C_2\lambda_2 + C_4\lambda_1 = 0, \\ C_1 \mathrm{ch}\lambda_2 L + C_2 \mathrm{sh}\lambda_2 L + C_3 \cos\lambda_1 L + C_4 \sin\lambda_1 L = 0, \\ \begin{cases} C_1\left(EI\lambda_2^3 \mathrm{sh}\lambda_2 L + \dfrac{1}{2}m\omega^2 ch\lambda_2 L\right) + C_2\left(EI\lambda_2^3 \mathrm{ch}\lambda_2 L + \dfrac{1}{2}m\omega^2 sh\lambda_2 L\right), \\ +C_3\left(EI\lambda_1^3 \sin\lambda_1 L + \dfrac{1}{2}m\omega^2 \cos\lambda_1 L\right) + C_4\left(\dfrac{1}{2}m\omega^2 \sin\lambda_1 L - EI\lambda_1^3 \cos\lambda_1 L\right) = 0. \end{cases} \end{cases} \tag{31}$$

This equation has a nonzero solution only if the determinant of the coefficients is equal to zero, i.e.,

$$\begin{vmatrix} 1 & 0 & 1 & 0 \\ 0 & \lambda_2 & 0 & \lambda_1 \\ \mathrm{ch}\lambda_2 L & \mathrm{sh}\lambda_2 L & \cos\lambda_1 L & \sin\lambda_1 L \\ \begin{cases} EI\lambda_2^3 \mathrm{sh}\lambda_2 L \\ +\frac{1}{2}m\omega^2 ch\lambda_2 L \end{cases} & \begin{cases} EI\lambda_2^3 \mathrm{ch}\lambda_2 L \\ +\frac{1}{2}m\omega^2 sh\lambda_2 L \end{cases} & \begin{cases} EI\lambda_1^3 \sin\lambda_1 L \\ +\frac{1}{2}m\omega^2 \cos\lambda_1 L \end{cases} & \begin{cases} \frac{1}{2}m\omega^2 \sin\lambda_1 L \\ -EI\lambda_1^3 \cos\lambda_1 L \end{cases} \end{vmatrix} = 0. \tag{32}$$

From this equation, the frequency equation for the antisymmetric mode functions can be written

$$\left(\lambda_1^3\lambda_2 - \lambda_1\lambda_2^3\right)\left(\cos\lambda_1 L \cdot \mathrm{ch}\lambda_2 L - 1\right) + \sin\lambda_1 L \cdot sh\lambda_2 L\left(\lambda_1^4 + \lambda_2^4\right) = 0. \tag{33}$$

Substituting Eq.(25) into (30) yields

$$\begin{cases} C_1 + C_3 = 0, \\ C_2\lambda_2 + C_4\lambda_1 = 0, \\ C_1\lambda_2 sh\lambda_2 L + C_2\lambda_2 ch\lambda_2 L - C_3\lambda_1 \sin\lambda_1 L + C_4\lambda_1 \cos\lambda_1 L = 0, \\ \begin{cases} C_1\left(EI\lambda_2^3 \mathrm{sh}\lambda_2 L + \frac{1}{2}m\omega^2 ch\lambda_2 L\right) + C_2\left(EI\lambda_2^3 \mathrm{ch}\lambda_2 L + \frac{1}{2}m\omega^2 sh\lambda_2 L\right) \\ +C_3\left(EI\lambda_1^3 \sin\lambda_1 L + \frac{1}{2}m\omega^2 \cos\lambda_1 L\right) + C_4\left(\frac{1}{2}m\omega^2 \sin\lambda_1 L - EI\lambda_1^3 \cos\lambda_1 L\right) = 0. \end{cases} \end{cases} \tag{34}$$

This equation also has a nonzero solution only if the determinant of the coefficients is equal to zero, i.e.,

$$\begin{vmatrix} 1 & 0 & 1 & 0 \\ 0 & \lambda_2 & 0 & \lambda_1 \\ \lambda_2 sh\lambda_2 L & \lambda_2 ch\lambda_2 L & -\lambda_1 \sin\lambda_1 L & \lambda_1 \cos\lambda_1 L \\ \begin{cases} EI\lambda_2^3 \mathrm{sh}\lambda_2 L \\ +\frac{1}{2}m\omega^2 ch\lambda_2 L \end{cases} & \begin{cases} EI\lambda_2^3 \mathrm{ch}\lambda_2 L \\ +\frac{1}{2}m\omega^2 sh\lambda_2 L \end{cases} & \begin{cases} EI\lambda_1^3 \sin\lambda_1 L \\ +\frac{1}{2}m\omega^2 \cos\lambda_1 L \end{cases} & \begin{cases} \frac{1}{2}m\omega^2 \sin\lambda_1 L \\ -EI\lambda_1^3 \cos\lambda_1 L \end{cases} \end{vmatrix} = 0. \tag{35}$$

It follows from this equation that the frequency equation for symmetric mode functions can be written

$$\begin{aligned} &EI\left(\lambda_1^4\lambda_2+\lambda_1^2\lambda_2^3\right)\sin\lambda_1 L\cdot ch\lambda_2 L\\ &\quad+EI\left(\lambda_1^3\lambda_2^2+\lambda_1\lambda_2^4\right)\cos\lambda_1 L\cdot sh\lambda_2 L\\ &\quad+\frac{1}{2}m\omega^2\left(\lambda_1^2-\lambda_2^2\right)\sin\lambda_1 L\cdot sh\lambda_2 L\\ &\quad+m\omega^2\lambda_1\lambda_2\left(\cos\lambda_1 L\cdot ch\lambda_2 L-1\right)=0. \end{aligned} \tag{36}$$

Eq.(21) can be simplified to

$$\begin{aligned} &q''+\omega^2 q+\left(\varepsilon A_1+\varepsilon A_2 q+\varepsilon A_3 q^2+\varepsilon A_4 q^3\right)q'\\ &\quad-\varepsilon A_5 q^2-\varepsilon A_6 q^3=0. \end{aligned} \tag{37}$$

Using the multiscale method, we can let

$$q=q_0(T_0,T_1,T_2)+\varepsilon q_1(T_0,T_1,T_2)+\varepsilon^2 q_2(T_0,T_1,T_2), \tag{38}$$

$$\omega^2=\omega_0^2\left(1+\varepsilon\sigma_1+\varepsilon^2\sigma_2+\cdots\right), \tag{39}$$

where $T_n=\varepsilon^n t\,(n=0,1,2,\ldots)$, $(d/dt)=D_0+\varepsilon D_1+\varepsilon^2 D_2$, $(d^2/dt^2)=D_0^2+2\varepsilon D_0D_1+\varepsilon^2(D_1^2+2D_0D_2)$.

Substituting Eq. (38) into (37) then yields

$$\begin{aligned} &\left[D_0^2+2\varepsilon D_0D_1+\varepsilon^2\left(D_1^2+2D_0D_2\right)\right]\left(q_0+\varepsilon q_1+\varepsilon^2 q_2\right)\\ &\quad+\omega_0^2\left(q_0+\varepsilon q_1+\varepsilon^2 q_2\right)\\ &+\left[\varepsilon A_1+\varepsilon A_2\left(q_0+\varepsilon q_1+\varepsilon^2 q_2\right)+\varepsilon A_3\left(q_0+\varepsilon q_1+\varepsilon^2 q_2\right)^2\right.\\ &\quad\left.+\varepsilon A_4\left(q_0+\varepsilon q_1+\varepsilon^2 q_2\right)^3\right]\left(D_0+\varepsilon D_1+\varepsilon^2 D_2\right)\left(q_0+\varepsilon q_1+\varepsilon^2 q_2\right)\\ &-\varepsilon A_5\left(q_0+\varepsilon q_1+\varepsilon^2 q_2\right)^2-\varepsilon A_6\left(q_0+\varepsilon q_1+\varepsilon^2 q_2\right)^3=0. \end{aligned} \tag{40}$$

Setting the sum of the coefficients of the parameter ε with the same power equal to zero yields

$$D_0^2q_0+\omega_0^2q_0=0, \tag{41a}$$

$$\begin{aligned} D_0^2q_1+\omega_0^2q_1=&-A_1D_0q_0-2D_0D_1q_0+A_5q_0^2-A_2D_0q_0^2\\ &+A_6q_0^3-A_3D_0q_0^3-A_4D_0q_0^4, \end{aligned} \tag{41b}$$

$$\begin{aligned} D_0^2q_2+\omega_0^2q_2=&-A_1D_1q_0-D_1^2q_0-2D_0D_2q_0-A_2D_1q_0^2\\ &-A_3D_1q_0^3-A_4D_1q_0^4-A_1D_0q_1\\ &-2D_0D_1q_1+2A_5q_0q_1-2A_2D_0q_0q_1\\ &+3A_6q_0^2q_1-3A_3D_0q_0^2q_1-4A_4D_0q_0^3q_1. \end{aligned} \tag{41c}$$

Solution of Eq.(41a) can be given as

$$q_0=A(T_1,T_2)e^{i\omega_0T_0}+\overline{A}(T_1,T_2)e^{-i\omega_0T_0}, \tag{42}$$

where A is an unknown function of a complex variable and $\overline{A}$is its complex conjugate.

Substituting Eq.(42) into Eq. (41b) yields

$$\begin{aligned} D_0^2q_1+\omega_0^2q_1=&\left(-A_1Ai\omega_0-2D_1Ai\omega_0-3A_3A^2\overline{A}i\omega_0+3A_6A^2\overline{A}\right)e^{i\omega_0T_0}\\ &+\left(A_5A^2-2A_2A^2i\omega_0-8A_4A^3\overline{A}i\omega_0\right)e^{2i\omega_0T_0}\\ &+\left(A_6A^3-3A_3A^3i\omega_0\right)e^{3i\omega_0T_0}\\ &-4A_4A^4i\omega_0e^{4i\omega_0T_0}\\ &+A_5A\overline{A}+CC, \end{aligned} \tag{43}$$

where CC is the complex conjugate of the previous term.

In order to eliminate the secular term in the equation, we let

$$-A_1Ai\omega_0-2D_1Ai\omega_0-3A_3A^2\overline{A}i\omega_0+3A_6A^2\overline{A}=0. \tag{44}$$

From this equation, it follows that

$$D_1A=-\frac{1}{2}A_1A-\frac{3}{2}A_3A^2\overline{A}+\frac{3A_6A^2\overline{A}}{2i\omega_0}. \tag{45}$$

Substituting Eq.(45) into Eq. (43) yields

$$\begin{aligned} q_1=&\left(\frac{2A_2A^2i\omega_0+8A_4A^3\overline{A}\,i\omega_0-A_5A^2}{3\omega_0^2}\right)e^{2i\omega_0T_0}\\ &+\left(\frac{3A_3A^3i\omega_0-A_6A^3}{8\omega_0^2}\right)e^{3i\omega_0T_0}\\ &\frac{4A_4A^4i}{15\omega_0}e^{4i\omega_0T_0}+\frac{A_5A\overline{A}}{\omega_0^2}+CC. \end{aligned} \tag{46}$$

Substituting Eqs. (42) and (46) into Eq. (41c) then yields

$$
\begin{aligned}
D_0^2 q_2 + \omega_0^2 q_2 = {} & \frac{112}{15} A^7 A_4^2 e^{7i\omega_0 T_0} + \left(\frac{24}{5} A^6 A_3 A_4 + \frac{4iA^6 A_4 A_6}{5\omega_0} - \frac{3iA^3 A_4 \left(3i\omega_0 A^3 A_3 - A^3 A_6\right)}{\omega_0} \right) e^{6i\omega_0 T_0} \\
& + \left(\frac{8}{3} A^5 A_2 A_4 + \frac{8iA^5 A_4 A_5}{15\omega_0} - \frac{15iA^2 A_3 \left(3i\omega_0 A^3 A_3 - A^3 A_6\right)}{8\omega_0} + \frac{3A^2 A_6 \left(3i\omega_0 A^3 A_3 - A^3 A_6\right)}{8\omega_0^2} - \frac{20iA^3 A_4 \left(2i\omega_0 A^2 A_2 - A^2 A_5 + 8i\omega_0 A^3 A_4 \overline{A}\right)}{3\omega_0} + 16A^6 A_4^2 \overline{A} \right) e^{5i\omega_0 T_0} \\
& + \left(\begin{array}{c} \frac{1}{2} A^4 A_1 A_4 - \frac{iAA_2 \left(3i\omega_0 A^3 A_3 - A^3 A_6\right)}{\omega_0} + \frac{AA_5 \left(3i\omega_0 A^3 A_3 - A^3 A_6\right)}{4\omega_0^2} + \frac{47}{10} A^5 A_3 A_4 \overline{A} - \frac{iA^5 A_4 A_6 \overline{A}}{10\omega_0} - \frac{6iA^2 A_4 \left(3i\omega_0 A^3 A_3 - A^3 A_6\right) \overline{A}}{\omega_0} \\ - \frac{4iA^2 A_3 \left(2i\omega_0 A^2 A_2 - A^2 A_5 + 8i\omega_0 A^3 A_4 \overline{A}\right)}{\omega_0} + \frac{A^2 A_6 \left(2i\omega_0 A^2 A_2 - A^2 A_5 + 8i\omega_0 A^3 A_4 \overline{A}\right)}{\omega_0^2} \end{array} \right) e^{4i\omega_0 T_0} \\
& + \left(\begin{array}{c} \frac{1}{2} A^3 A_1 A_3 - \frac{15}{8} A^4 A_3^2 \overline{A} + \frac{8}{5} A^4 A_2 A_4 \overline{A} - \frac{352iA^4 A_4 A_5 \overline{A}}{15\omega_0} - \frac{3iA^4 A_3 A_6 \overline{A}}{\omega_0} + \frac{9A^4 A_6^2 \overline{A}}{8\omega_0^2} - \frac{9iAA_3 \left(3i\omega_0 A^3 A_3 - A^3 A_6\right) \overline{A}}{4\omega_0} + \frac{3AA_6 \left(3i\omega_0 A^3 A_3 - A^3 A_6\right) \overline{A}}{4\omega_0^2} \\ + \frac{48}{5} A^5 A_4^2 \overline{A}^2 - \frac{2iAA_2 \left(2i\omega_0 A^2 A_2 - A^2 A_5 + 8i\omega_0 A^3 A_4 \overline{A}\right)}{\omega_0} + \frac{2AA_5 \left(2i\omega_0 A^2 A_2 - A^2 A_5 + 8i\omega_0 A^3 A_4 \overline{A}\right)}{3\omega_0^2} - \frac{12iA^2 A_4 \overline{A} \left(2i\omega_0 A^2 A_2 - A^2 A_5 + 8i\omega_0 A^3 A_4 \overline{A}\right)}{\omega_0} \end{array} \right) e^{3i\omega_0 T_0} \\
& + \left(\begin{array}{c} \frac{1}{2} A^2 A_1 A_2 - \frac{5}{2} A^3 A_2 A_3 \overline{A} + 2A^3 A_1 A_4 \overline{A} - \frac{14iA^3 A_3 A_5 \overline{A}}{\omega_0} - \frac{5iA^3 A_2 A_6 \overline{A}}{2\omega_0} + \frac{8A^3 A_5 A_6 \overline{A}}{\omega_0^2} - \frac{iA_2 \left(3i\omega_0 A^3 A_3 - A^3 A_6\right) \overline{A}}{2\omega_0} + \frac{A_5 \left(3i\omega_0 A^3 A_3 - A^3 A_6\right) \overline{A}}{4\omega_0^2} \\ - \frac{42}{5} A^4 A_3 A_4 \overline{A}^2 - \frac{46iA^4 A_4 A_6 \overline{A}^2}{5\omega_0} - \frac{3iAA_4 \left(3i\omega_0 A^3 A_3 - A^3 A_6\right) \overline{A}^2}{\omega_0} - \frac{4iAA_3 \overline{A} \left(2i\omega_0 A^2 A_2 - A^2 A_5 + 8i\omega_0 A^3 A_4 \overline{A}\right)}{\omega_0} + \frac{2AA_6 \overline{A} \left(2i\omega_0 A^2 A_2 - A^2 A_5 + 8i\omega_0 A^3 A_4 \overline{A}\right)}{\omega_0^2} \end{array} \right) e^{2i\omega_0 T_0} \\
& + \frac{1}{4} A_1 A_2 A \overline{A} + \frac{3}{4} A_2 A_3 A^2 \overline{A}^2 + \frac{3}{4} A_1 A_4 A^2 \overline{A}^2 + \frac{3iA_2 A_6 A^2 \overline{A}^2}{4\omega_0} + \frac{6A_5 A_6 A^2 \overline{A}^2}{\omega_0^2} + \frac{9}{4} A_3 A_4 A^3 \overline{A}^3 + \frac{9iA_4 A_6 A^3 \overline{A}^3}{4\omega_0} + \frac{A_6 \overline{A}^2 \left(2i\omega_0 A^2 A_2 - A^2 A_5 + 8i\omega_0 A_4 A^3 \overline{A}\right)}{\omega_0^2} + \mathrm{CC.}
\end{aligned}
\tag{47}
$$

In order to eliminate the secular term in this equation, we can set the coefficient of the term $e^{i\omega_0 T_0}$ to be zero:

$$
\begin{aligned}
& 240 D_2 A \omega^3 + 30 A_1^2 A i\omega^2 + 160 A_2^2 A^2 \overline{A} i\omega^2 + 180 A_1 A_3 A^2 \overline{A} i\omega^2 + 240 A_2 A_5 A^2 \overline{A} \omega \\
& + 400 A_5^2 A^2 \overline{A} i + 405 A_3^2 \overline{A}^2 A^3 i\omega^2 + 1280 A_2 A_4 A^3 \overline{A}^2 i\omega^2 + 1600 A_4 A_5 A^3 \overline{A}^2 \omega \\
& - 180 A_3 A_6 A^3 \overline{A}^2 \omega + 225 A_6^2 A^3 \overline{A}^2 i + 2688 A_4^2 A^4 \overline{A}^3 i\omega^2 = 0.
\end{aligned}
\tag{48}
$$

From this equation, it can be concluded that

$$
\begin{aligned}
D_2 A = {} & -\frac{iAA_1^2}{8\omega_0} - \frac{2iA^2 A_2^2 \overline{A}}{3\omega_0} - \frac{3iA^2 A_1 A_3 \overline{A}}{4\omega_0} - \frac{A^2 A_2 A_5 \overline{A}}{\omega_0^2} - \frac{5iA^2 A_5^2 \overline{A}}{3\omega_0^3} - \frac{27iA^3 A_3^2 \overline{A}^2}{16\omega_0} \\
& - \frac{16iA^3 A_2 A_4 \overline{A}^2}{3\omega_0} - \frac{20A^3 A_4 A_5 \overline{A}^2}{3\omega_0^2} + \frac{3A^3 A_3 A_6 \overline{A}^2}{4\omega_0^2} - \frac{15iA^3 A_6^2 \overline{A}^2}{16\omega_0^3} - \frac{56iA^4 A_4^2 \overline{A}^3}{5\omega_0}.
\end{aligned}
\tag{49}
$$

Substituting Eq. (49) into Eq. (47) then yields

$$
\begin{aligned}
q_2 = & -\frac{7A^7A_4^2}{45\omega_0^2}e^{7i\omega_0T_0} - \left(\frac{69A^6A_3A_4}{175\omega_0^2} + \frac{19iA^6A_4A_6}{175\omega_0^3}\right)e^{6i\omega_0T_0} \\
& + \left(-\frac{15A^5A_3^2}{64\omega_0^2} - \frac{2A^5A_2A_4}{3\omega_0^2} - \frac{3iA^5A_4A_5}{10\omega_0^3} - \frac{iA^5A_3A_6}{8\omega_0^3} + \frac{A^5A_6^2}{64\omega_0^4} - \frac{26A^6A_4^2\overline{A}}{9\omega_0^2}\right)e^{5i\omega_0T_0} \\
& + \left(-\frac{11A^4A_2A_3}{15\omega_0^2} - \frac{A^4A_1A_4}{30\omega_0^2} - \frac{19iA^4A_3A_5}{60\omega_0^3} - \frac{iA^4A_2A_6}{5\omega_0^3} + \frac{A^4A_5A_6}{12\omega_0^4} - \frac{547A^5A_3A_4\overline{A}}{150\omega_0^2} - \frac{139iA^5A_4A_6\overline{A}}{150\omega_0^3}\right)e^{4i\omega_0T_0} \\
& + \left(\begin{array}{c} -\frac{A^3A_2^2}{2\omega_0^2} - \frac{A^3A_1A_3}{16\omega_0^2} - \frac{5iA^3A_2A_5}{12\omega_0^3} + \frac{A^3A_5^2}{12\omega_0^4} - \frac{39A^4A_3^2\overline{A}}{64\omega_0^2} - \frac{26A^4A_2A_4\overline{A}}{5\omega_0^2} \\ + \frac{23iA^4A_4A_5\overline{A}}{30\omega_0^3} - \frac{3iA^4A_3A_6\overline{A}}{16\omega_0^3} - \frac{3A^4A_6^2\overline{A}}{64\omega_0^4} - \frac{66A^5A_4^2\overline{A}^2}{5\omega_0^2} \end{array}\right)e^{3i\omega_0T_0} \\
& + \left(\begin{array}{c} -\frac{A^2A_1A_2}{6\omega_0^2} - \frac{7A^3A_2A_3\overline{A}}{3\omega_0^2} - \frac{2A^3A_1A_4\overline{A}}{3\omega_0^2} + \frac{37iA^3A_3A_5\overline{A}}{12\omega_0^3} - \frac{2iA^3A_2A_6\overline{A}}{3\omega_0^2} \\ - \frac{23A^3A_5A_6\overline{A}}{12\omega_0^4} - \frac{163A^4A_3A_4\overline{A}^2}{15\omega_0^2} - \frac{49iA^4A_4A_6\overline{A}^2}{15\omega_0^3} \end{array}\right)e^{2i\omega_0T_0} \\
& + \frac{5A^2A_5A_6\overline{A}^2}{\omega_0^4} + \frac{AA_1A_2\overline{A}}{4\omega_0^2} + \frac{3A^2A_2A_3\overline{A}^2}{4\omega_0^2} + \frac{3A^2A_1A_4\overline{A}^2}{4\omega_0^2} + \frac{9A^3A_3A_4\overline{A}^3}{4\omega_0^2} + \frac{11iA^2A_2A_6\overline{A}^2}{4\omega_0^3} + \frac{41iA^3A_4A_6\overline{A}^3}{4\omega_0^3} + \text{CC.}
\end{aligned}
\tag{50}
$$

Here

$$
\frac{dA}{dt} = D_0A + \varepsilon D_1A + \varepsilon^2 D_2A, \tag{51}
$$

where $D_0A = 0$.

Substituting Eqs.(45) and (49) into Eq. (51) yields

$$
\begin{aligned}
\frac{dA}{dt} = & \varepsilon\left(-\frac{1}{2}A_1A - \frac{3}{2}A_3A^2\overline{A} + \frac{3A_6A^2\overline{A}}{2i\omega_0}\right) \\
& + \varepsilon^2\left(\begin{array}{c} -\frac{iAA_1^2}{8\omega_0} - \frac{2iA^2A_2^2\overline{A}}{3\omega_0} - \frac{3iA^2A_1A_3\overline{A}}{4\omega_0} - \frac{A^2A_2A_5\overline{A}}{\omega_0^2} - \frac{5iA^2A_5^2\overline{A}}{3\omega_0^3} - \frac{27iA^3A_3^2\overline{A}^2}{16\omega_0} \\ - \frac{16iA^3A_2A_4\overline{A}^2}{3\omega_0} - \frac{20A^3A_4A_5\overline{A}^2}{3\omega_0^2} + \frac{3A^3A_3A_6\overline{A}^2}{4\omega_0^2} - \frac{15iA^3A_6^2\overline{A}^2}{16\omega_0^3} - \frac{56iA^4A_4^2\overline{A}^3}{5\omega_0} \end{array}\right).
\end{aligned}
\tag{52}
$$

We then write

$$
A(t) = \frac{1}{2}K(t)e^{i\theta(t)}, \tag{53}
$$

where $K(t)$ and $\theta(t)$ are time-varying functions.

Substituting Eq. (53) into Eq. (52) yields

$$K' = -\frac{1}{2}A_1 K\varepsilon - \frac{3}{8}A_3 K^3\varepsilon - \frac{A_2A_5K^3\varepsilon^2}{4\omega_0^2} - \frac{5A_4A_5K^5\varepsilon^2}{12\omega_0^2} + \frac{3A_3A_6K^5\varepsilon^2}{64\omega_0^2}, \tag{54}$$

$$\theta' = -\frac{5A_5^2K^2\varepsilon^2}{12\omega_0^3} - \frac{15A_6^2K^4\varepsilon^2}{256\omega_0^3} - \frac{3A_6K^2\varepsilon}{8\omega_0} - \frac{A_1^2\varepsilon^2}{8\omega_0} - \frac{A_2^2K^2\varepsilon^2}{6\omega_0} - \frac{3A_1A_3K^2\varepsilon^2}{16\omega_0} - \frac{27A_3^2K^4\varepsilon^2}{256\omega_0} - \frac{A_2A_4K^4\varepsilon^2}{3\omega_0} - \frac{7A_4^2K^6\varepsilon^2}{40\omega_0}. \tag{55}$$

Substituting Eqs. (42), (46), and (50) into Eq. (38) yields

$$q(t) = K\cos\varphi + \varepsilon\begin{pmatrix} -\frac{A_5}{6\omega_0^2}K^2\cos 2\varphi - \frac{A_2}{3\omega_0}K^2\sin 2\varphi - \frac{A_4}{3\omega_0}K^4\sin 2\varphi - \frac{A_6}{32\omega_0^2}K^3\cos 3\varphi \\ -\frac{3A_3}{32\omega_0}K^3\sin 3\varphi - \frac{A_4}{30\omega_0}K^4\sin 4\varphi + \frac{A_5}{2\omega_0^2}K^2 \end{pmatrix}$$

$$+\varepsilon^2\begin{pmatrix} -\frac{A_1A_2}{12\omega_0^2}K^2\cos 2\varphi - \frac{7A_2A_3}{24\omega_0^2}K^4\cos 2\varphi - \frac{A_1A_4}{12\omega_0^2}K^4\cos 2\varphi - \frac{163A_3A_4}{480\omega_0^2}K^6\cos 2\varphi \\ -\frac{37A_3A_5}{96\omega_0^3}K^4\sin 2\varphi + \frac{A_2A_6}{12\omega_0^3}K^4\sin 2\varphi + \frac{49A_4A_6}{480\omega_0^3}K^6\sin 2\varphi - \frac{23A_5A_6}{96\omega_0^4}K^4\cos 2\varphi \\ -\frac{A_2^2}{8\omega_0^2}K^3\cos 3\varphi - \frac{A_1A_3}{64\omega_0^2}K^3\cos 3\varphi - \frac{39A_3^2}{1024\omega_0^2}K^5\cos 3\varphi - \frac{13A_2A_4}{40\omega_0^2}K^5\cos 3\varphi \\ -\frac{33A_4^2}{160\omega_0^2}K^7\cos 3\varphi + \frac{5A_2A_5}{48\omega_0^3}K^3\sin 3\varphi - \frac{23A_4A_5}{480\omega_0^3}K^5\sin 3\varphi + \frac{3A_3A_6}{256\omega_0^3}K^5\sin 3\varphi \\ +\frac{A_5^2}{48\omega_0^4}K^3\cos 3\varphi - \frac{3A_6^2}{1024\omega_0^4}K^5\cos 3\varphi - \frac{11A_2A_3}{120\omega_0^2}K^4\cos 4\varphi - \frac{A_1A_4}{240\omega_0^2}K^4\cos 4\varphi \\ -\frac{547A_3A_4}{4800\omega_0^2}K^6\cos 4\varphi + \frac{19A_3A_5}{480\omega_0^3}K^4\sin 4\varphi + \frac{A_2A_6}{40\omega_0^3}K^4\sin 4\varphi + \frac{139A_4A_6}{4800\omega_0^3}K^6\sin 4\varphi \\ +\frac{A_5A_6}{96\omega_0^4}K^4\cos 4\varphi - \frac{15A_3^2}{1024\omega_0^2}K^5\cos 5\varphi - \frac{A_2A_4}{24\omega_0^2}K^5\cos 5\varphi - \frac{13A_4^2}{288\omega_0^2}K^7\cos 5\varphi \\ +\frac{3A_4A_5}{160\omega_0^3}K^5\sin 5\varphi + \frac{A_3A_6}{128\omega_0^3}K^5\sin 5\varphi + \frac{A_6^2}{1024\omega_0^4}K^5\cos 5\varphi - \frac{69A_3A_4}{5600\omega_0^2}K^6\cos 6\varphi \\ +\frac{19A_4A_6}{5600\omega_0^3}K^6\sin 6\varphi - \frac{7A_4^2}{2880\omega_0^2}K^7\cos 7\varphi + \frac{5A_5A_6}{8\omega_0^4}K^4 + \frac{A_1A_2}{8\omega_0^2}K^2 + \frac{3A_2A_3}{32\omega_0^2}K^4 \\ +\frac{3A_1A_4}{32\omega_0^2}K^4 + \frac{9A_3A_4}{128\omega_0^2}K^6 \end{pmatrix}, \tag{56}$$

where $\varphi = \theta + t\omega_0$, and K and θ can be determined by Eqs.(54) and (55).

Thus, the nonlinear resonant frequency of the sensor can be found from Eq.(39) to be

$$\omega = \omega_0 \sqrt{1 - \varepsilon \frac{3A_6K^2}{4} - \varepsilon^2 \left(\begin{array}{c} \dfrac{A_1^2}{4} + \left(\dfrac{A_2^2}{3} + \dfrac{3A_1A_3}{8} + \dfrac{5A_5^2}{6} \right) K^2 \\ + \left(\dfrac{27A_3^2}{128} + \dfrac{2A_2A_4}{3} - \dfrac{3A_6^2}{128} \right) K^4 + \dfrac{7A_4^2}{20} K^6 \end{array} \right) + \cdots}. \tag{57}$$

The pressure sensor structure is shown in Figure 3(a) The pressure membrane used for detecting the pressure is a rectangular membrane fixed at four edges. Here, P denotes the pressure applied to the membrane, and L_f denotes its length and its width. The sizes of the membrane are shown in Figure 3(b).

If we let d denote the thickness of the pressure membrane and w denote its elastic displacement, the boundary conditions of the pressure membrane can be written as

$$\begin{cases} w|_{x=\pm L_f} = w|_{y=\pm L_f} = 0, \\ \left.\dfrac{\partial w}{\partial x}\right|_{x=\pm L_f} = \left.\dfrac{\partial w}{\partial y}\right|_{y=\pm L_f} = 0. \end{cases} \tag{58}$$

The elastic displacement of the pressure membrane satisfying all boundary conditions is then

$$w = A_{11}\left(1 + \cos\left(\frac{\pi x}{L_f}\right)\right)\left(1 + \cos\left(\frac{\pi y}{L_f}\right)\right). \tag{59}$$

Substituting Eq. (59) into the Galerkin equation yields

$$\int\int \left(P - D\nabla^4 w\right)\left(1 + \cos\left(\frac{\pi x}{L_f}\right)\right)\left(1 + \cos\left(\frac{\pi y}{L_f}\right)\right)\mathrm{d}x\mathrm{d}y = 0. \tag{60}$$

From Eq. (60), it follows that

$$A_{11} = \frac{PL_f^4}{2\pi^4 D}, \tag{61}$$

where $D = Ed^3/12(1-\mu^2)$.

The relationship between displacement and stress is known as follows:

$$\sigma_x = -\frac{Ez}{1-\mu^2}\left(\frac{\partial^2 w}{\partial x^2} + \mu\frac{\partial^2 w}{\partial y^2}\right). \tag{62}$$

Substituting Eq. (59) into Eq. (62) yields

$$\sigma_x = \frac{EzA_{11}\pi^2}{1-\mu^2}\left[\frac{1}{L_f^2}\cos\frac{\pi x}{L_f}\left(1 + \cos\frac{\pi y}{L_f}\right) + \frac{\mu^2}{L_f^2}\cos\frac{\pi y}{L_f}\left(1 + \cos\frac{\pi x}{L_f}\right)\right]. \tag{63}$$

At $y = 0$ and $z = d/2$, the stress on the pressure membrane is

$$\left.\sigma_x\right|_{\substack{y=0 \\ z=(d/2)}} = \frac{3P}{\pi^2}\left(\frac{L_f}{d}\right)^2\left[(2+\mu)\cos\frac{\pi x}{L_f} + \mu\right]. \tag{64}$$

Its average value can be written

$$\begin{aligned} \overline{\sigma}_x &= \frac{3P}{\pi^2}\left(\frac{L_f}{d}\right)^2 \frac{\int_0^{L_f}\left[(2+\mu)\cos\left(\pi x/L_f\right) + \mu\right]\mathrm{d}x}{L_f} \\ &= 3P\left(\frac{L_f}{\pi d}\right)^2 \mu. \end{aligned} \tag{65}$$

Thus, the axial force F in the resonator is

$$F = 3P\left(\frac{L_f}{\pi d}\right)^2 \mu \times h \times L_f. \tag{66}$$

When Eq. (66) is substituted into Eq. (18), the effects of the gas pressure on the sensor can be determined.

4. Results and Discussion

By using a cross-type resonator, the area of capacitance electrode between the resonator and the substrate is increased, and the capacitance variation is increased under the same resonator vibration amplitude, that is, the strength of the resonant signal of the microresonant pressure sensor is increased.

Comparison between the traditional resonator and the cross-type resonator is given in Table 1. Here, S is the pole area, $\Delta\overline{y}$ is the average vibration amplitude, ΔC is the capacitance change, and U_{out} is the output signal voltage. Table 2 shows parameters of the sensor system, and Figures 4 and 5 show effects of nonlinear parameter on resonant frequencies and resonant frequency difference.

The pole area of the cross-type resonator is 1.5 times of the traditional resonator. So, the capacitance change and the output signal voltage of the cross-type resonator are about 2 times of the traditional resonator. It is very beneficial to the design and manufacture of the signal-processing circuit.

The chosen parameters of the resonator are shown in Table 2. Here, the material is silicon (Si), and the nonlinear parameter is $\varepsilon = 0.25$ when other parameters are changed. $\varepsilon = y_0/d_0$ is the ratio of the static displacement of the resonator to initial clearance. If $\varepsilon = y_0/d_0$ is above 0.3, the resonator will come into instability state. So, the nonlinear

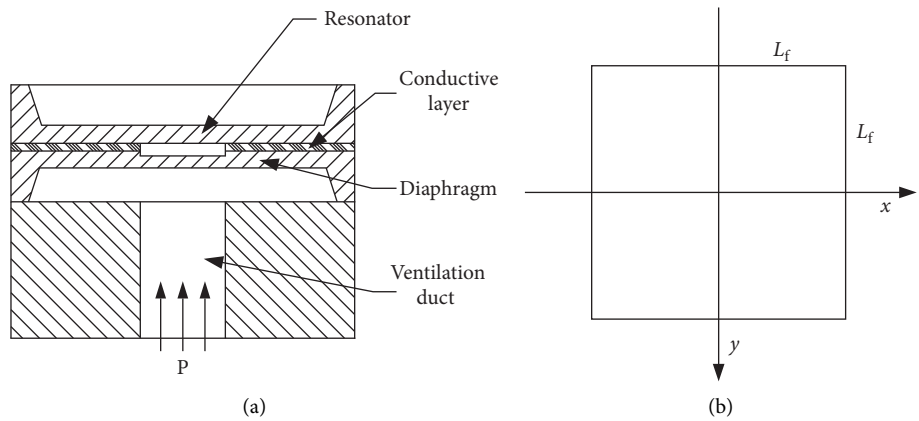

Figure 3: Structure and sizes of the pressure sensor (a) sensor structure (b) sizes of the pressure membrane.

Table 1: Comparison between traditional and cross-type resonators.

	S/m^2	$\Delta\bar{y}/m$	$\Delta C/F$	U_{out}/mV
Traditional resonator	9.6×10^{-7}	2.0870×10^{-7}	1.4315×10^{-11}	103.330
Cross-type resonator	14.4×10^{-7}	2.5584×10^{-7}	2.9446×10^{-11}	220.064
times	1.50	1.23	2.06	2.13

Table 2: Parameters of the sensor system.

L (m)	b (m)	h (m)	m (kg)	E (GPa)	ρ (kg/m^3)
4×10^{-3}	5×10^{-4}	1×10^{-5}	3.495×10^{-8}	190	2330
ε_0 ($C^2{\cdot}N^{-1}m^{-2}$)	ε_r	U_0 (V)	d_0 (m)	H_v (J)	F (N)
8.85×10^{-12}	1	1.0	5×10^{-7}	10×10^{-19}	1

Table 3: Comparison of linear and nonlinear resonant frequencies for the first four orders.

Odd mode function			
	ω_0 (Hz)	ω_1 (Hz)	η (%)
Mode (1, 1)	35388.10	33054.06	6.596
Mode (2, 2)	74560.91	72885.34	2.004
Mode (3, 3)	114017.01	113038.15	0.859
Mode (4, 4)	154808.42	154115.23	0.448
Even mode function			
	ω_0 (Hz)	ω_1 (Hz)	η (%)
Mode (1, 1)	44117.75	42588.68	3.534
Mode (2, 2)	80909.60	79886.53	1.265
Mode (3, 3)	120061.71	119279.67	0.651
Mode (4, 4)	161300.35	160673.29	0.389

parameter is taken to be 0.25. Using Eqs. (36) and (57), the linear and nonlinear frequencies of the first four orders of resonant vibration of the resonant sensor are obtained, as shown in Table 3.

Effects of the nonlinear parameter and molecular force on the nonlinear frequencies and the difference between the linear and nonlinear frequencies were investigated (see Figures 4–6). Here ω_0 is the linear resonant frequency, ω_1 is the nonlinear resonant frequency, $\Delta\omega_a$ is the difference between the linear and nonlinear resonant frequencies considering molecular force, $\Delta\omega_b$ is the difference between the linear and nonlinear resonant frequencies without considering molecular force, and η is the relative difference between the linear and nonlinear resonant frequencies. The following can be deduced from Table 3 and Figures 4–6:

(1) The nonlinear resonant frequency is lower than the linear resonant frequency. This shows that nonlinearity has the property of a soft spring. The frequency difference between the linear and nonlinear resonant frequencies decreases gradually from low-order to high-order modes. The frequency difference for the first-order mode is about 13 times that of the fourth-order mode.

(2) The resonant frequency difference of the odd-number order modes is about twice that of the even-number order modes. As the order number increases, the resonant frequency difference for the odd-number modes gradually approaches one for the even-number modes. From Eq.(21), it is known that the nonlinear effects are related to the coefficients A_1, A_2, A_3, A_4, A_5, and A_6, which depend on the vibration modes of the resonator. For the odd-number order modes, these coefficients are larger than those of the even order modes. So, the nonlinearity has more obvious effects on the odd-

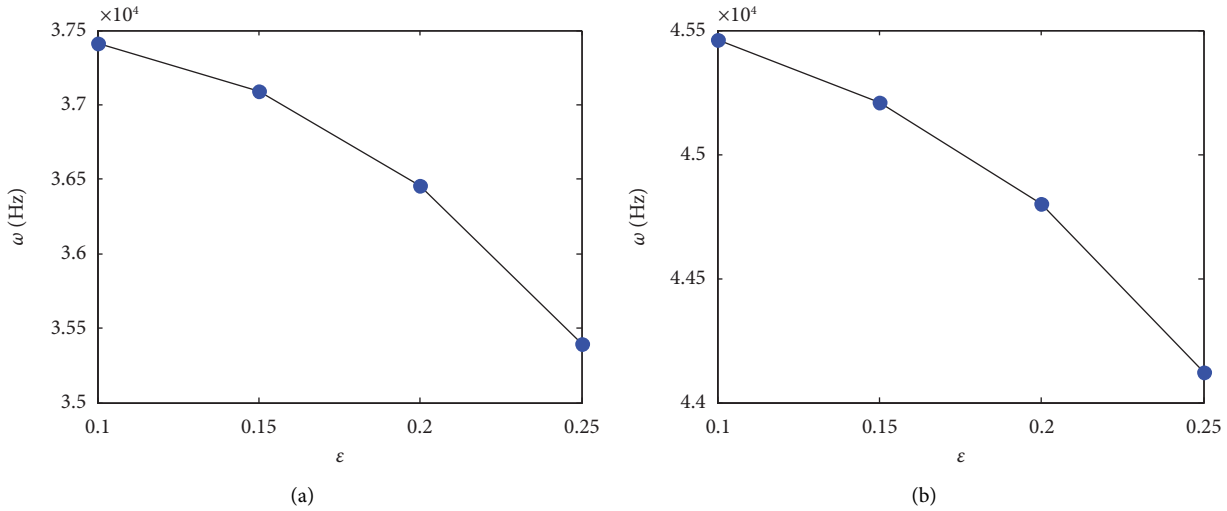

Figure 4: Effects of the nonlinear parameter on resonant frequencies. (a) Odd. (b) Even.

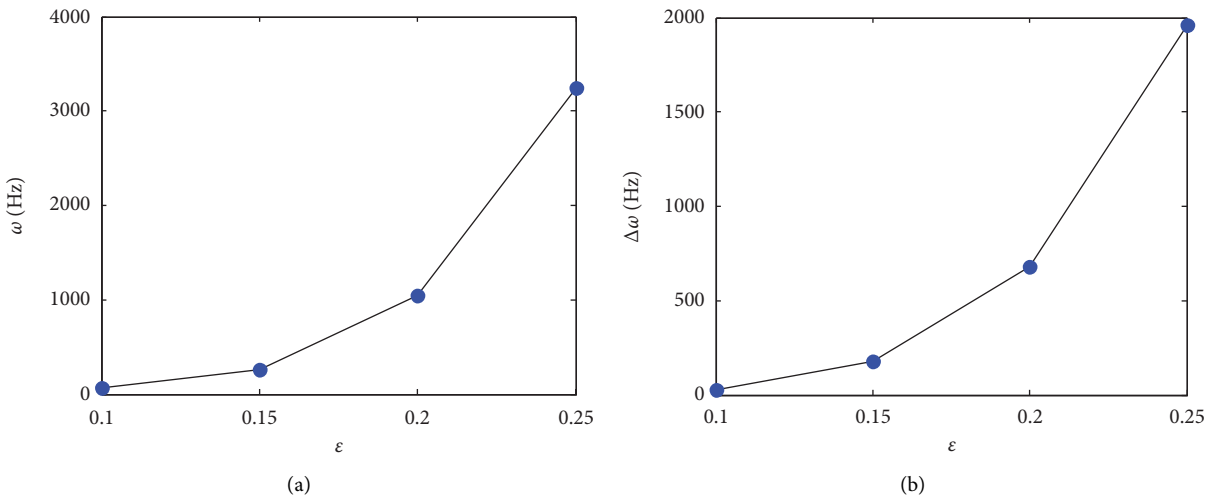

Figure 5: Effects of the nonlinear parameter on resonant frequency difference. (a) Odd. (b) Even.

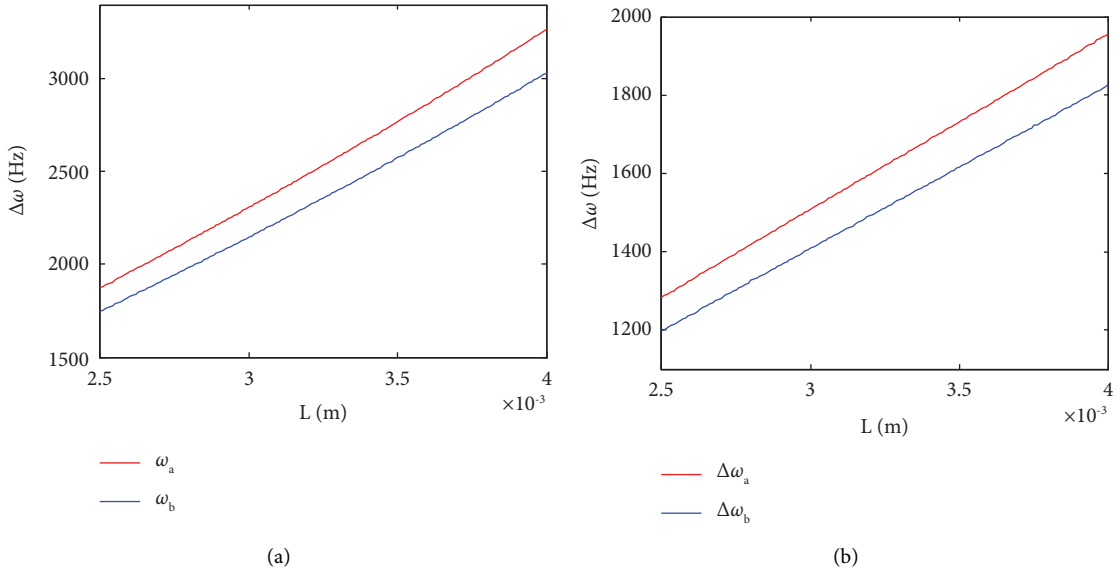

Figure 6: Effects of molecule force and resonator length on resonant frequency difference. (a) Odd. (b) Even.

number order modes than those on the even-number order modes.

(3) With an increase of the nonlinear parameter ε, the nonlinear resonant frequencies decrease. When the nonlinear parameter ε increases from 0.1 to 0.25, the resonant frequency of the odd-number order mode decreases by 5.3%, and the resonant frequency of the even-number order mode decreases by 2.9%. The nonlinear parameter has a more obvious effect on the resonant frequencies for the odd-number order modes than that for the even-number order modes. With an increase of the nonlinear parameter ε, the frequency difference between the linear and nonlinear resonant frequencies increases gradually as well. For odd-number order modes, the frequency difference increases more significantly than for the even-number order modes.

(4) The difference between the linear and nonlinear resonant frequencies is larger when molecular force is considered than when it is not considered. The frequency difference for the odd-number order modes is larger than for the even-number order modes. As the length of the resonator increases, the frequency difference between the linear and nonlinear resonant frequencies increases gradually. This means that the effect of the molecular force on the resonant frequencies increases along with the resonator length.

By changing the length and thickness of the resonator and the clearance between the resonator and the base plane, the variation of resonant frequencies with and without considering nonlinearity can be further studied. The results are shown in Figures 7–10.

(1) With an increase in the length of the resonator, its resonant frequency decreases, and the decrease of high-order resonant frequencies is more evident than those of low order. When the length of the resonator increases from 2.5×10^{-3} to 4×10^{-3} m, the resonant frequency of the first odd-number order decreases by 16.6%, while the resonant frequency of the fourth odd-number order decreases by 39.3%. At the same time, the resonant frequency of the first even-number order decreases by 19.8%, while the resonant frequency of the fourth even-number order decreases by 42.2%.

With an increase in the length of the resonator, the frequency difference between the linear and nonlinear resonant frequencies increases. This means that effects of the nonlinearity on the resonant frequencies increase as the resonator length increases. For the odd-number modes, the effects of the nonlinearity are more significant than those for the even-number modes.

(2) With an increase in the clearance between the resonator and the base plane, the resonant frequency increases, and the increases of the low-order resonant frequencies are more obvious than those of the high-order modes. When the clearance increases from 3×10^{-7} m to 4.5×10^{-7} m, the first odd-number order resonant frequency increases by 6.53% and the fourth odd-number order resonant frequency increases by 0.35%. At the same time, the first even-number order resonant frequency increases by 3.50% and the fourth even-number order resonant frequency increases by 0.29%. With an increase of the clearance between the resonator and the base plane, the frequency difference between the linear and nonlinear resonant frequencies decreases. This means that effects of the nonlinearity on the resonant frequencies decreases as the clearance between the resonator and the base plane decreases.

(3) With an increase in the thickness of the resonator, its resonant frequency decreases, and the decrease of the high-order resonant frequency is more significant than that of the low-order modes. As the thickness of the resonator increases from 2×10^{-6} m to 10×10^{-6} m, the resonant frequency of the first-order mode decreases by 48.5%, while the resonant frequency of the fourth-order mode decreases by only about 1/4 as much. With an increase of the thickness of the resonator, the frequency difference between the linear and nonlinear resonant frequencies decreases. This means that effects of the nonlinearity on the resonant frequencies decrease as the resonator thickness decreases.

In brief: the effects of the nonlinearity on the resonant frequencies increase for larger length, smaller clearance, and smaller thickness.

Effects of the pressure on the resonant frequencies for the sensor have been investigated and are shown in Figures 11 and 12. Here are conclusions that can be drawn:

With an increase of gas pressure, the resonant frequencies increase, and the increase of the high-order resonant frequencies is greater than that of the low-order modes. When the gas pressure increases from 0 to 3×10^5 Pa, the resonant frequency of the first odd-number order increases by 77.8% and the resonant frequency of the fourth odd-number order decreases by 116.7%. At the same time, the resonant frequency of the first even-number order increases by 78.95%, and the resonant frequency of the fourth even-number order decreases by 142.11%. As the gas pressure increases, the frequency difference between the linear and nonlinear resonant frequencies decreases. For the low-order modes, effects of the gas pressure on the resonant frequency and the resonant-frequency differences are more significant than for the high-order modes. This means that effects of the nonlinearity on the resonant frequencies decrease as the pressure decreases. For the even-number modes, the effects of the pressure are more significant than for the odd-number modes.

In brief: with increasing gas pressure, the resonant frequency of the resonator increases, effects of the nonlinearity on the resonant frequency weaken, and effects of the gas

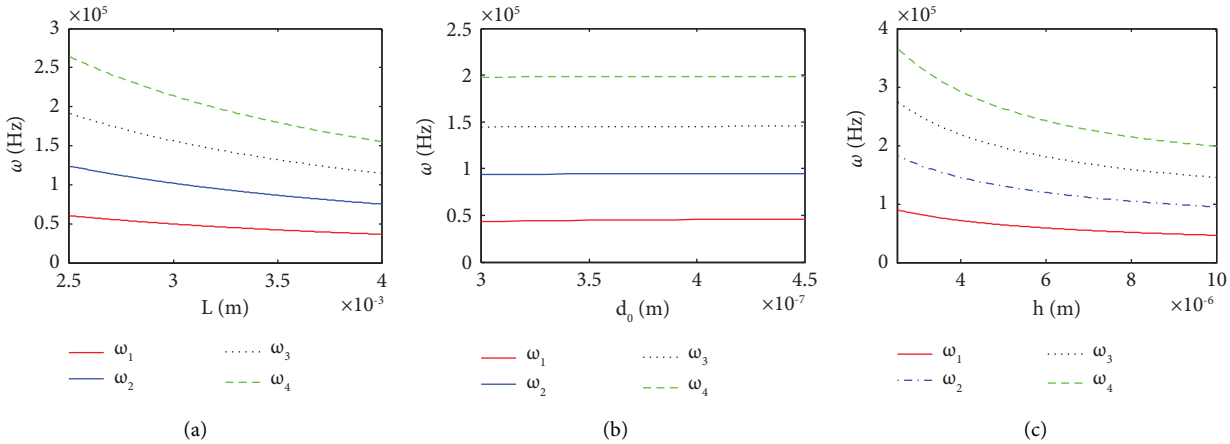

FIGURE 7: Changes of the resonant frequencies with system parameters (odd modes) (a) length changes (b) clearance changes (c) thickness changes.

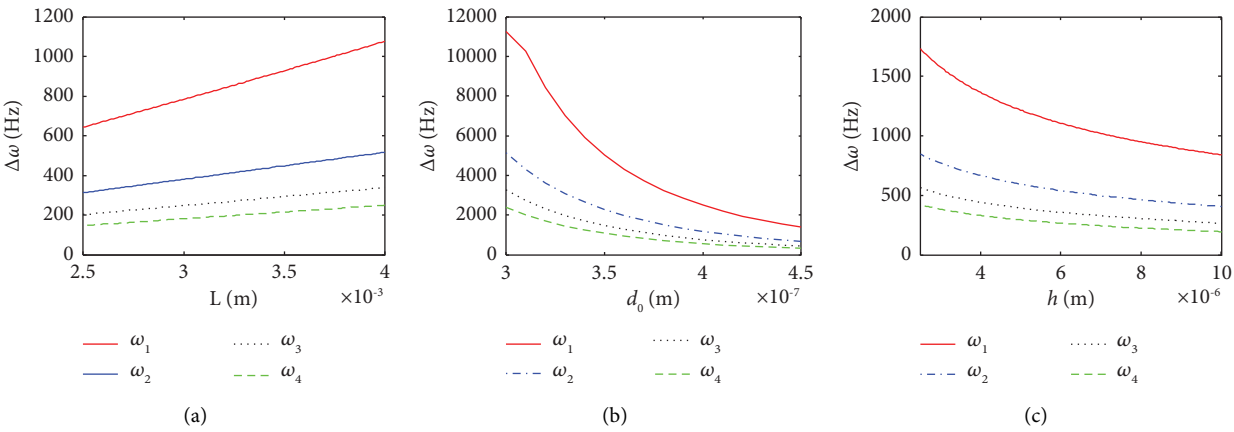

FIGURE 8: Changes of the resonant frequency differences with system parameters (odd modes) (a) length changes (b) clearance changes (c) thickness changes.

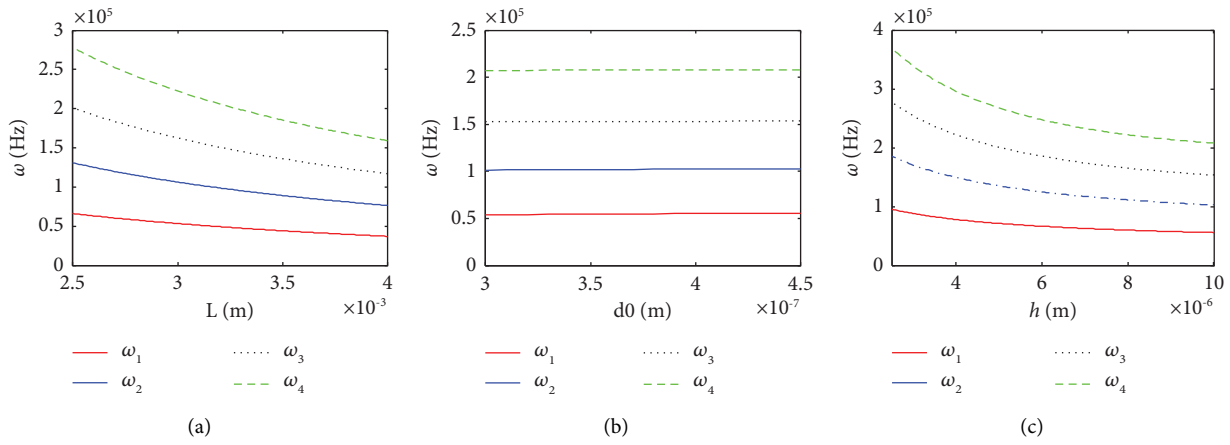

FIGURE 9: Changes of the resonant frequencies with system parameters (even modes) (a) length changes (b) clearance changes (c) thickness changes.

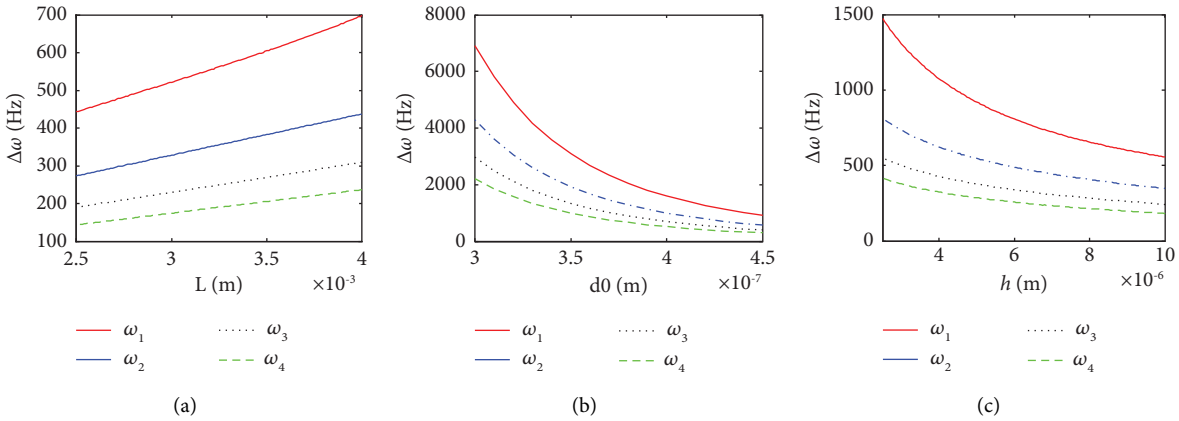

FIGURE 10: Changes of the resonant frequency differences with system parameters (even modes). From these figures, the following conclusions can be reached: (a) length changes (b) clearance changes (c) thickness changes.

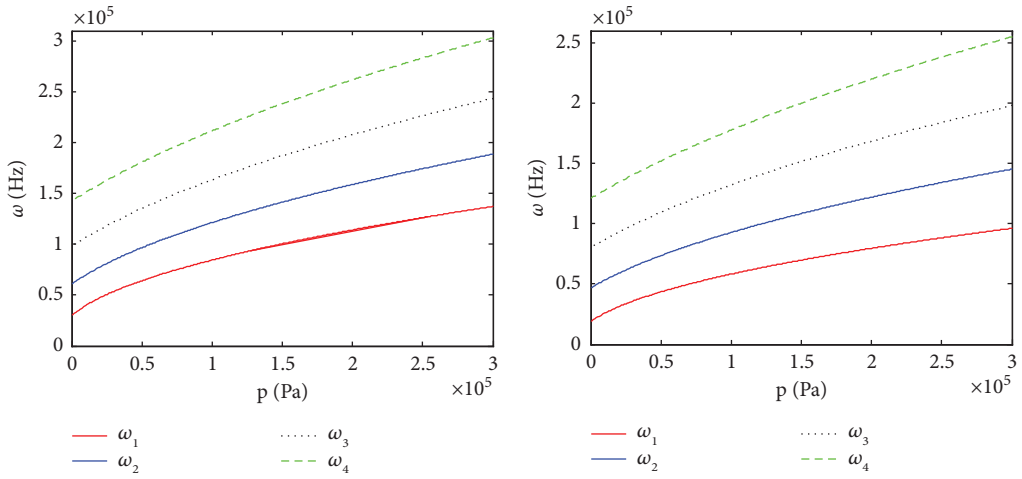

FIGURE 11: Changes of the resonant frequencies with pressure (a) odd modes (b) even modes.

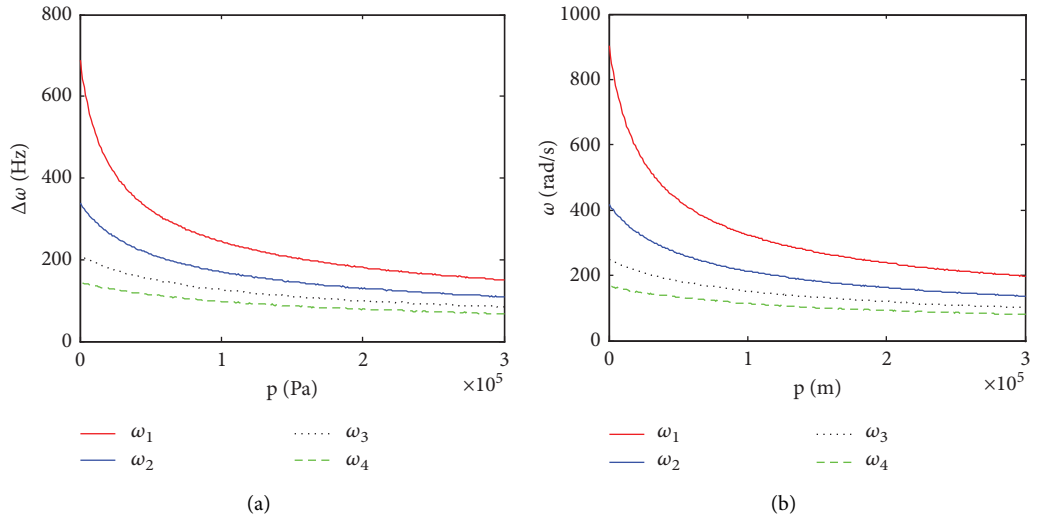

FIGURE 12: Changes of the resonant frequency differences with pressure (a) odd modes (b) even modes.

Table 4: Comparison of the multiscale method and the numerical method.

	Odd mode function		
	ω_1 (Hz)	ω_2 (Hz)	η_2 (%)
Mode (1, 1)	33054.06	33988.17	2.826
Mode (2, 2)	72885.34	74654.99	2.428
Mode (3, 3)	113038.15	115868.63	2.504
Mode (4, 4)	154115.23	157837.11	2.415
	Even mode function		
	ω_1 (Hz)	ω_2 (Hz)	η_2 (%)
Mode (1, 1)	42588.68	43686.38	2.577
Mode (2, 2)	79886.53	82704.93	3.528
Mode (3, 3)	119279.67	122441.77	2.651
Mode (4, 4)	160673.29	164764.03	2.546

pressure on the resonant frequency are more significant for the even-number modes than for the odd-number modes.

Using software MATLAB, Dsolve function is used to resolve the differential equation (37), and the nonlinear resonant frequencies are obtained. The results are shown in Table 4. Here, ω_2 is the nonlinear resonant frequencies obtained by Dsolve function, and η_2 is the relative error between the numerical simulations and the multiscale method. Results show that the maximum relative error between the nonlinear resonant frequencies given by the numerical simulations and the multiscale method is 3.528%. It illustrates the multiscale method in the research.

5. Conclusions

In this paper, a nonlinear dynamics equation for a novel microresonant pressure sensor is proposed. Effects of the system parameters and gas pressure on the nonlinear resonant frequencies are investigated. Results show the following conclusions:

(1) The nonlinear resonant frequency is less than the linear resonant frequency. The frequency difference between the linear and nonlinear resonant frequencies decreases gradually from low-order to high-order modes.

(2) The frequency difference between the linear and nonlinear resonant frequencies is larger when molecular force is considered than when it is not considered.

(3) The effects of the nonlinearity on the resonant frequencies increase with increasing resonator length or decreasing the clearance between the resonator and the baseplate. With increasing gas pressure, the resonant frequency of the resonator increases.

Data Availability

The data used to support the findings of this study are included within the article.

Conflicts of Interest

The authors declare that they have no conflicts of interest.

References

[1] B. S. Kim, J. S. Park, B. Hun Kang, and C. Moon, "Fabrication and property analysis of a MEMS micro-gripper for robotic micro-manipulation," *Robotics and Computer-Integrated Manufacturing*, vol. 28, no. 1, pp. 50–56, 2012.

[2] D. Wang, X. Gu, J. Xie, and D. Zhang, "Research on a Ka-band MEMS power sensor investigated with an MEMS cantilever beam," *Chinese Journal of Electronics*, vol. 29, no. 2, pp. 378–384, 2020.

[3] S. Duan, W. Wang, S. Zhang, X. Yang, Y. Zhang, and G. Zhang, "A bionic MEMS electronic stethoscope with double-sided diaphragm packaging," *IEEE Access*, vol. 9, pp. 27122–27129, 2021.

[4] V. Britcher and S. Bergbreiter, "Use of a MEMS differential pressure sensor to detect ground, ceiling, and walls on small quadrotors," *IEEE Robotics and Automation Letters*, vol. 6, no. 3, pp. 4568–4575, 2021.

[5] N. G. Rafael, M. B. Anna, and D. Alfons, "AC transfer function of electrostatic capacitive sensors based on the ID. equivalent model: application to silicon microphones," *Journal of Microelectromechanical Systems*, vol. 12, pp. 972–978, 2003.

[6] Y. Wan, Y. Pan, and J. Huang, "Some countries/regions support initiatives to promote MEMS development," *Modern Manufacturing Engineering*, vol. 5, pp. 135–139, 2012.

[7] S. Santosh Kumar and A. Tanwar, "Development of a MEMS-based barometric pressure sensor for micro air vehicle (MAV) altitude measurement," *Microsystem Technologies*, vol. 26, no. 3, pp. 901–912, 2020.

[8] P. Schmitt and M. Hoffmann, "Engineering a compliant mechanical amplifier for MEMS sensor applications," *Journal of Microelectromechanical Systems*, vol. 29, no. 2, pp. 214–227, 2020.

[9] D. Lange, C. Hagleitner, A. Hierlemann, O. Brand, and H. Baltes, "Complementary metal oxide semiconductor cantilever arrays on a single chip:mass-sen-sitive detection of volatile organic compounds," *Analytical Chemistry*, vol. 74, no. 13, pp. 3084–3095, 2002.

[10] M. R. Werner and W. Fahrner, "Review on materials, micro sensors, systems, and devices for high-temperature and harsh-environment applications," *IEEE Transactions on Industrial Electronics*, vol. 48, no. 2, pp. 249–257, 2001.

[11] X. Han, L. Zhao, J. Wang et al., "High-accuracy differential resonant pressure sensor with linear fitting method," *Journal of Micromechanics and Microengineering*, vol. 31, no. 4, Article ID 045006, 2021.

[12] Y. Li, C. Cheng, Y. Lu et al., "A high-sensitivity resonant differential pressure microsensor based on bulk micromachining," *IEEE Sensors Journal*, vol. 21, no. 7, pp. 8927–8934, 2021.

[13] X. Shi, S. Zhang, D. Chen et al., "A resonant pressure sensor based upon electrostatically comb driven and piezoresistively sensed lateral resonators," *Micromachines*, vol. 10, no. 7, p. 460, 2019.

[14] Z. Li, S. Fan, and L. Cheng, "A graphene resonant pressure sensor with an optical fiber F-P cavity," *Metrology & Measurement Technology*, vol. 39, pp. 36–39, 2019.

[15] S. Matej, A. Bradesko, D. Belavic, A. Bencan, B. Malic, and T. Rojac, "Construction and functionality of a ceramic resonant pressure sensor for operation at elevated temperatures," *Sensors*, vol. 18, no. 5, p. 1423, 2018.

[16] S. Zhang, Y. Zheng, Y. Lu et al., "A micromachined resonant micro-pressure sensor," *IEEE Sensors Journal*, vol. 21, no. 18, p. 1, 2021.
[17] C. Xiang, Y. Lu, C. Cheng, J. Wang, D. Chen, and J. Chen, "A resonant pressure microsensor with a wide pressure measurement range," *Micromachines*, vol. 12, no. 4, p. 382, 2021.
[18] L. Zhao, X. Han, Q. Mao et al., "Temperature-insensitive silicon resonant pressure sensor by thermal stress control," *Sensors and Actuators A: Physical*, vol. 322, Article ID 112612, 2021.
[19] P. Yan, Y. Lu, C. Xiang, J. Wang, D. Chen, and J. Chen, "A temperature-insensitive resonant pressure micro sensor based on silicon-on-glass vacuum packaging," *Sensors*, vol. 19, no. 18, p. 3866, 2019.
[20] M. Zamanzadeh, I. Jafarsadeghi-Pournaki, and H. M. Ouakad, "A resonant pressure MEMS sensor based on levitation force excitation detection," *Nonlinear Dynamics*, vol. 100, no. 2, pp. 1105–1123, 2020.
[21] X. Han, Q. Mao, L. Zhao et al., "Novel resonant pressure sensor based on piezoresistive detection and symmetrical in-plane mode vibration," *Microsyst. Nanoeng.,* vol. 6, no. 1, p. 95, 2020.
[22] D. Mata-Hernandez, D. Fernández, S. Banerji, and J. Madrenas, "Resonant MEMS pressure sensor in 180 nm CMOS technology obtained by BEOL isotropic etching," *Sensors*, vol. 20, no. 21, p. 6037, 2020.
[23] N. Alcheikh, A. Z. Hajjaj, and M. I. Younis, "Highly sensitive and wide-range resonant pressure sensor based on the veering phenomenon," *Sensors and Actuators A: Physical*, vol. 300, Article ID 111652, 2019.
[24] G. Han, X. Fu, and L. Xu, "Free vibration for a micro resonant pressure sensor with cross-type resonator," *Advances in Mechanical Engineering*, vol. 13, no. 1, Article ID 168781402098733, 2021.
[25] Q. Li, S. Fan, Z. Tang, and W. Xing, "Non-linear dynamics of an electrothermally excited resonant pressure sensor," *Sensors and Actuators A: Physical*, vol. 188, pp. 19–28, 2012.
[26] F. Zhang, A. Li, Z. Bu et al., "Vibration modes interference in the MEMS resonant pressure sensor," *International Journal of Modern Physics B*, vol. 31, no. 29, Article ID 1750223, 2017.
[27] X. Fu and L. Xu, "Vibrations of a resonant gas sensor under multicoupled fields," *Journal of Computational and Nonlinear Dynamics*, vol. 14, no. 4, Article ID 041002, 2019.
[28] X. Fu and L. Xu, "Multi-field coupled chaotic vibration for a micro resonant pressure sensor," *Applied Mathematical Modelling*, vol. 72, pp. 470–485, 2019.
[29] S. Schmid, L. G. Villanueva, and M. L. Roukes, *Fundamentals of Nanomechanical Resonators*, Springer International Publishing, Cham, Switzerland, 2016.
[30] R. W. Fox and F. M. White, *Introduction to Fluid Mechanics*, John Wiley & Sons, New York, NY, USA, 1992.
[31] S. A. Zhou, "On forces in microelectromechanical systems," *International Journal of Engineering Science*, vol. 41, no. 3-5, pp. 313–335, 2003.
[32] L. Z. Xu and Q. Yang, "Multi-field coupled dynamics for a micro beam," *Mechanics Based Design of Structures and Machines*, vol. 43, no. 1, pp. 57–73, 2015.